Atomic-scale design of friction and energy dissipation

Antonio Cammarata,[1,*] Paolo Nicolini,[1,†] Kosta Simonovic,[1] Egor Ukraintsev,[1,2] and Tomas Polcar[1]
[1]*Faculty of Electrical Engineering, Czech Technical University in Prague, Technicka 2, 16627 Prague 6, Czech Republic*
[2]*Institute of Physics of the Czech Academy of Sciences, Department of Thin Films and Nanostructures, Cukrovarnicka 10, 16200 Prague 6, Czech Republic*

(Received 16 November 2018; revised manuscript received 13 March 2019; published 25 March 2019)

Study of friction and energy dissipation always relied on direct observations. Actual theories provide limited prediction on the frictional and dissipative properties if only the material chemistry and geometry are known. We here develop a framework to study intrinsic friction and energy dissipation based on the only knowledge of the normal modes of the system at equilibrium. We derive an approximated expression for the first anharmonic term in the potential energy expansion which does not require the computation of the third-order force constants. Moreover, we show how to characterize the frequency content of observed physical quantities and individuate the dissipative processes active during experimental measurements. As a case study, we consider the relative sliding motion of atomic layers in molybdenum disulfide dry lubricant, and we discuss how to extract information on the energetics of sliding from atomic force microscopy signals. The presented framework switches the investigation paradigm on friction and energy dissipation from dynamic to static studies, paving avenues to explore for the design of alternative anisotropic tribological and thermal materials.

DOI: 10.1103/PhysRevB.99.094309

I. INTRODUCTION

Friction is a phenomenon that has an immense impact in our everyday life. It can be generally defined as the set of forces that oppose the relative motion of two bodies. It can have beneficial effects (e.g., without friction we would not be able to walk), but it is in general considered as a detrimental phenomenon. As a matter of fact, when two bodies are in relative motion, frictional forces do work. Since this quantity is deeply connected to the irreversibility of the process, it is also referred to as *dissipated* work. Friction has been studied for centuries; these efforts led to the formulation of the well-known Amontons' laws of friction. These laws apply at the macroscopic scale, while at the atomistic level a more detailed description needs to be adopted. An old but still very popular model for understanding friction, in particular stick-slip dynamics, is the one proposed by Prandtl [1] and Tomlinson [2]. In such a model, a point mass m is dragged by a spring of force constant k over a periodic potential of maximum amplitude V_0 and periodicity a while a viscous force of damping coefficient γ is acting on the mass [3]. The power of this model consists on the fact that, with only a few simple physical ingredients, one can characterize the transition from stick-slip to smooth dynamics observed at nanoscale [4] by means of defining a dimensionless parameter. The model has been improved since its invention, for example, by adding thermal noise to it [5] or going beyond the monodimensional description [6]. The Prandtl-Tomlinson model is indeed useful for interpreting lateral-force-versus-displacement profiles observed at nanoscale, but it cannot provide an *a priori* estimation of the energy loss due to friction. In fact, the dissipated work depends directly on the explicit values of the set parameters and not all of them can be obtained easily. The periodicity a is generally known, and, in the case of sliding experiments with atomic force microscopy (AFM), the value of the spring constant can also be quickly measured. Computational approaches can be employed for estimating shape and amplitude of the underlying potential [7]. The damping parameter γ is the most subtle one to estimate; often scientists study the limit cases of under- and over-damped regimes [8]. Moreover, since the viscous term represents the average damping behavior of the system, such a description may be inadequate to model materials that present anisotropic dissipation behaviors. Finally, it has to be stressed that both the thermal noise (if included in the model) and the damping term arise from interactions with phonons and/or other fast excitations that are not included explicitly [8].

In this work we make some step toward the development of a description aimed at taking directly into account such dissipation channels. We present a general framework that can be readily used to estimate dissipative properties directly, by using the atomic types and the geometry of the stable state only. Within the present description, we focus on the atomic friction phenomenology, disregarding then any mechanical deformation (like puckering or wrinkling effects) which will change the geometry and/or the connectivity of the stable state. To exemplify the methodology, we will apply our atomic-scale description of dissipation to study the specific case of sliding in molybdenum disulfide, which is regarded as a prototypical dry lubricant and widely studied for its peculiar properties, ranging from macroscopic tribological contact [9], to nanoelectronics [10], to catalysis [11]. We will show how to identify and potentially control the dissipation channels in terms of phonon-phonon coupling. Within this

*cammaant@fel.cvut.cz
†nicolpao@fel.cvut.cz

contribution, we will consider dissipative processes involving phonons only, leaving the extension of the discussion to other source of dissipation for future works.

II. COMPUTATIONAL AND EXPERIMENTAL DETAILS

A. Molecular dynamics simulations

All molecular dynamics (MD) simulations were performed using the LAMMPS package [12] and the force field reported elsewhere [13]. After retrieving the structure obtained with x-ray diffraction [14], a bilayer system in a slab configuration (i.e., adding 20 Å vacuum above the top layer) was prepared by replicating the primitive cell six and three times in the *a* and *b* crystallographic directions, respectively (i.e., the final supercell contains 106 atoms). The structure optimization also allowing the box sizes to relax was performed by using the conjugate gradient method. Subsequently, the system was equilibrated for 50 ps using a Nosé-Hoover [15,16] chain of thermostats. Two sets of simulations were then carried out; in the first case we started the molecular dynamics trajectory adding a speed of 750 m/s to the atoms belonging to the top layer. In the second set, two rigid bodies encompassing the topmost and bottommost sulfur layers respectively were defined. Sliding simulations were performed by keeping fixed the position of the bottommost sulfur layer and by imposing a constant speed of 1 m/s to the topmost one. All sliding simulations were carried out in the NVE ensemble. A timestep of 0.1 fs was employed for all simulations. We computed phonon eigenvectors and eigenfrequencies with the aid of the PHONOPY software [17].

B. MoS_2 deposition

MoS_2 coatings were deposited on mirror polished (Ra = 0.52 nm) Silicon (Si) substrates using AJA Orion 4 plasma vapour deposition chamber (AJA, U.S.A.). Before the deposition, substrates were sonicated for 30 min in each of the following solutions: isopropanol, *n*-heptane and isopropanol. After the sonication, samples were dried in a stream of hot air and placed into the deposition chamber. Finally, before the deposition process began, samples were plasma etched for 1 h in Argon plasma with Ar^+ pressure equal to 0.13 kPa. Power and bias voltage were set to 30 W and 47 V, respectively. MoS_2 coating was sputtered from MoS_2 target (99 weight % purity, Able targets limited, China) in D.C. regime using the Ar^+ plasma as working gas. Deposition parameters were the following: power on target 80 W, bias voltage 128 V, Ar^+ gas pressure 0.39 kPa, temperature 773 K, deposition time 1 h.

C. Atomic force microscopy experiment

Tribological experiments were done with the NT-MDT Ntegra atomic force microscope in the lateral force mode. Untreated, uncoated CSG01 AFM cantilever was slid over the sputtered MoS_2 sample. Although, the AFM tip is made out of silicon, transfer of MoS_2 on to the Si tip is well known and described in the literature [18–22]; hence, we can safely assume that in the performed experiment we have indeed observed a MoS_2-MoS_2 contact. To obtain a clear AFM signal, both the tip and the sample were immersed into a liquid cell filled with deionized water [23,24]. The stiffness of the tip was obtained through the Sader method [25,26] and was equal to 0.057 N/m. The vertical drift of the signal due to the soft cantilever was automatically corrected during the acquisition. Dynamic measurements were performed with a load of 2.7 nN and a linear sliding speed of 13.6 nm/s (0.33 Hz sliding frequency), in which the lateral force signal was recorded on a 20 × 20 nm portion of the sample recording 2000 data points per line. Only a fraction of the acquired data was necessary for the numerical analysis.

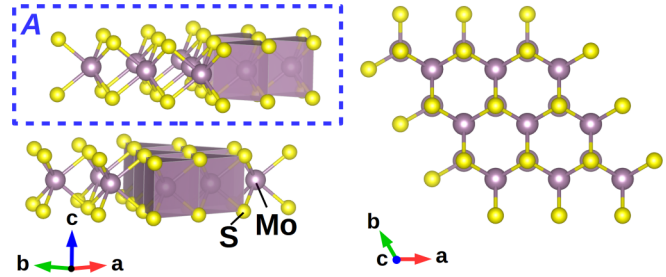

FIG. 1. Hexagonal $P6_3/mmc$ structure of 2H polymorph MoS_2 bulk compound. Mo–S bonds are arranged in a trigonal prismatic coordination forming MoS_2 layers that can reciprocally slide thanks to weak van der Waals interactions. The set of atoms forming the *A* layer considered in our analysis is indicated with a blue-dashed rectangle.

III. RESULTS

A. Mode decomposition of sliding trajectories

The MoS_2 crystalline compound owns a layered structure, with each layer formed by hexagonally packed Mo atoms forming covalent bonds with six chalcogen S anions in a trigonal prismatic coordination (Fig. 1); adjacent layers are coupled by weak van der Waals forces that allow them to slide promptly. We select the 2H polymorph crystalline MoS_2 structure with hexagonal $P6_3/mmc$ symmetry (SG 194) [14], which has been shown to correspond to the the most stable geometry among several arrangements of adjacent MoS_2 layers [7]. We then build our model geometry by considering only two subsequent layers along the axis orthogonal to the layer plane and add a vacuum region by expanding the corresponding dimension of the simulation box. To investigate which are the atomic-scale processes responsible of the nanoscale friction we focus on the set of atoms forming one of the two layers (set *A*—Fig. 1). Our main aim is to relate the friction response, which is a dynamic property, to intrinsic static features of the system. We already saw [27–30] that a promising and viable way is to describe the sliding motion in terms of the phonon modes of the stable system. In this perspective, we will exploit the knowledge of the set of the polarization eigenvectors at the Γ point [31] of the Brillouin zone in the following way: (i) define a sliding direction $\boldsymbol{d}$ and the set *A*; (ii) select a phonon mode *j* and consider the relative displacement vectors associated to each atom of the *A* layer; (iii) calculate the resulting displacement vector $\boldsymbol{r}_j$ of the center of mass of the layer; (iv) consider the scalar product $r_{j\perp\boldsymbol{d}} = \boldsymbol{r}_j \cdot \boldsymbol{d}$; (v) iterate (ii–iv) by considering all the eigenvectors at

Γ, once at a time, and finally (vi) select the modes with the highest projection. We observe that the majority of the modes have projection $r_{j\perp \boldsymbol{d}}$ lower than 0.4×10^{-10} Å^2, while only six modes have projection higher than 0.1×10^{-3} Å^2, those being Γ(4), Γ(5), Γ(113), Γ(114), Γ(208), and Γ(209) (see Sec. S1 in the Supplemental Material [32]). We will refer to them as *sliding modes* of the A layer, because they have an effective geometric contribution to the layer drift along the direction $\boldsymbol{d}$. The algorithm we outlined above to identify the sliding modes is based only on geometric arguments; indeed, we will now show that the sliding modes play an active role in the energetics of the layer drift.

B. Anharmonic effects

The layer sliding is geometrically represented by a sequence of atomic positions which can be far from the equilibrium configuration. To study the energetics of the system during sliding we must then consider anharmonic effects, such as phonon-phonon scattering, and how these determine the redistribution of the total energy among the phonon modes. To this aim, we include the first anharmonic term in the Taylor expansion of the potential energy, written as a sum of phonon contributions:

$$V = \frac{1}{2}\sum_j \omega_j^2 |Q_j|^2 + \frac{1}{6}\sum_{j,j',j''} \Phi_{jj'j''} |Q_j||Q_{j'}||Q_{j''}|, \qquad (1)$$

where $\Phi_{jj'j''}$ is the strength of interaction [33] between the three phonons j, j', and j'' involved in the scattering. The detail of the formalism shown in this section is reported in the Secs. S2 and S3 in the Supplemental Material [32]. By solving the Euler-Lagrange equations of the phonon system, we then obtain the equation of motion of each phonon coordinate Q_j:

$$\ddot{Q}_j + \frac{1}{2}\Phi_{jjj}Q_j^2 + \left(\omega_j^2 + \sum_{j'\neq j}\Phi_{jjj'}Q_{j'}\right)Q_j + \frac{1}{2}\sum_{j',j''\neq j}\Phi_{jj'j''}Q_{j'}Q_{j''} = 0. \qquad (2)$$

The presence of the term $\omega_j^2 Q_j$ in Eq. (2), and the fact that if $\Phi_{jj'j''} = 0$ for each triad, such equation reduces to the equation of the harmonic oscillator, suggest that each normal coordinate Q_j can be written as a sum of a harmonic Q_j^H and anharmonic Q_j^{an} term:

$$Q_j = Q_j^H + Q_j^{\mathrm{an}}, \qquad (3)$$

with $Q_j^H = C_j e^{i\omega_j t}$ being the solution of the harmonic oscillator equation. With this choice, the acceleration $\ddot{Q}_j$ of the normal coordinate Q_j can be written as a sum of different contributions from harmonic and anharmonic terms containing:

(1) $Q_j^H \propto \cos(\omega_j t)$, oscillating at frequency ω_j,

(2) $(Q_j^H)^2 \propto \cos^2(\omega_j t)$, oscillating at frequency $2\omega_j$,

(3) $Q_j^H \sum_{j'\neq j}\Phi_{jjj'}Q_{j'}^H \propto \cos(\omega_j t)\cos(\omega_{j'} t)$, oscillating at frequencies $\omega_j + \omega_{j'}$ and $\omega_j - \omega_{j'}$,

(4) $\sum_{j',j''\neq j}\Phi_{jj'j''}Q_{j'}^H Q_{j''}^H \propto \cos(\omega_{j'} t)\cos(\omega_{j''} t)$, oscillating at frequencies $\omega_{j'} + \omega_{j''}$ and $\omega_{j'} - \omega_{j''}$.

By means of the transformation done in Eq. (3), it is then possible to characterize the spectral components of all the simulated physical quantities by assigning each frequency to a specific phonon-phonon scattering process.

According to Eq. (2), the study of anharmonic effects requires the knowledge of the interaction strength $\boldsymbol{\Phi}$; however, if some of the coupling contributions can be neglected, the potential energy V in Eq. (1) can be approximated as

$$V \approx \frac{1}{3}\sum_j \omega_j^2 |Q_j|^2 + \frac{1}{3}\sum_j \frac{1}{\omega_j^2}|\ddot{Q}_j|^2; \qquad (4)$$

in other words, it is enough to calculate the projection of the atomic forces onto the phonon modes to get the mode accelerations $\ddot{Q}_j$ and hence the potential energy, and no information is needed about the interaction strength matrix $\boldsymbol{\Phi}$. This considerably reduces the computational effort especially in quantum mechanical simulations, in which the calculation of the $\Phi_{jj'j''}$ elements can be prohibitive even for moderate size systems (∼100 atoms). Indeed, we find that our approximation in Eq. (4) reproduces well the potential energy even far from the minima, with small deviations only in proximity of some maxima (see the Sec. S3 of the Supplemental Material [32]). The total energy E, including the first anharmonic contribution to the potential, can then be decomposed as a sum of contribution from each normal mode in the same fashion as in the harmonic approximation:

$$E \approx \frac{1}{2}\sum_j |\dot{Q}_j|^2 + \frac{1}{3}\sum_j \left(\omega_j^2 |Q_j|^2 + \frac{1}{\omega_j^2}|\ddot{Q}_j|^2\right), \qquad (5)$$

where the sum runs over all the j system modes.

As a final comment, it is here worthy to note that assumptions represented by Eqs. (3) and (4) are independent and can be separately exploited to study the phonon-phonon coupling.

C. Frictional response: From dynamic to static calculations

The study of friction always relied on both dynamic experimental and simulation studies, since friction produces dissipation phenomena as a response to external stimuli which do not take place instantaneously. We will now show that such dynamic studies are not necessary and information on friction can be obtained from static simulations.

To present a case study, we performed 15 molecular dynamics simulations in the NVE ensemble using the MoS_2 bilayer geometry showed in Fig. 1, where the layer A has a nonnull initial drift velocity along the x axis in our setting ($[\boldsymbol{d} = (1, 0, 0)]$ and the initial system temperature is 0, 50, 75, 100, 125, 150, 200, 250, 300, 350, 400, 500, 600, 700, 800 K, respectively. In this set of simulations, no thermal bath is coupled to the system, therefore energy cannot be exchanged with the environment. As we will show below, dissipative processes can nevertheless take place through internal redistribution of energy during the dynamics. To show this, we then consider the position vector of the center of mass of the layer A along the trajectory and project it onto the sliding direction $\boldsymbol{d}$; at the same time, we use Eq. (5) to calculate the energy E_{sl} of only the sliding modes j_{sl}. We observe that, irrespective of the temperature, E_{sl} is oscillating between maxima and minima due to the continuous energy transfer to and from the remaining phonon modes of the system. However, after some oscillations, the value of E_{sl} decreases with the time; once the

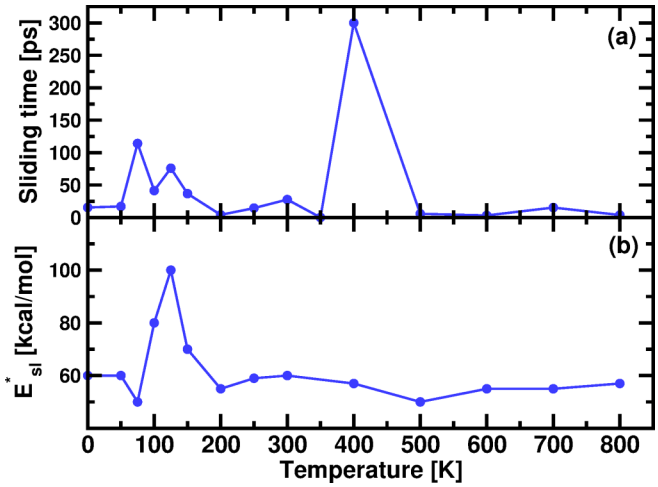

FIG. 2. (a) Sliding time and (b) critical sliding energy $E^*_{\rm sl}$ of the layer A as a function of the temperature. Despite the initial velocity has been chosen to be the same in all the simulations, no clear dependence with the temperature is found. Since no sliding has been observed at $T = 350$ K, the corresponding $E^*_{\rm sl}$ is missing. Lines are a guide for the eye.

maximum value is definitely below a critical threshold $E^*_{\rm sl}$, then the sliding stops and the system reaches the equilibrium. The initial velocity of the layer A has been chosen to be the same in all simulations; however, the sliding time and the critical value $E^*_{\rm sl}$ have no monotonic relation with the temperature of the system (Fig. 2). This is a clear indication that the sliding time depends on the details of the system configuration at the beginning of the simulation, such as atom velocity distribution and phonon population, and how these evolve with the time. A closer inspection of the system dynamics is then needed. To this aim, the oscillating behavior of $E_{\rm sl}$ and the decomposition in Eq. (5) suggest considering the Fourier transform of the total energy E calculated at each time t along the entire trajectory, at each of the considered temperature values [Fig. 3(a)]. We observe that both the kinetic and the potential energy are characterized by well-defined frequency contributions irrespective of the temperature. A close inspection shows that some of the peaks occur in correspondence of the eigenfrequencies of phonon modes, including the sliding ones. It is worth noting that the total energy here considered is the one calculated during the molecular dynamics simulation and no approximation is applied. The frequency spectra showed in Fig. 3(a) display extra peaks besides those coming from the fundamental vibrations of the systems. Such extra peaks are due to anharmonic effects: As a result of the scattering among harmonic phonons, new phonons are created with frequencies different than the fundamental ones. The assignment of the frequencies other than the harmonic ones can be done by means of the approximated solution [Eq. (3)]. The main anharmonic contributions are of the kind $\omega_j \pm \omega_{j'}$, where ω_j and $\omega_{j'}$ are the harmonic eigenfrequencies; we are then able to assign each anharmonic peak to a specific phonon recombination process. After this assignment, we see that the main anharmonic peaks involve both sliding modes and others different than the sliding ones. The phonon recombination processes are responsible of the energy transfer (interactions) among the harmonic phonons: If such processes involve sliding and nonsliding modes, then the layer decelerates until it stops. From now on, we will refer to such nonsliding modes as the *dissipative* ones. The study of the frictional force is

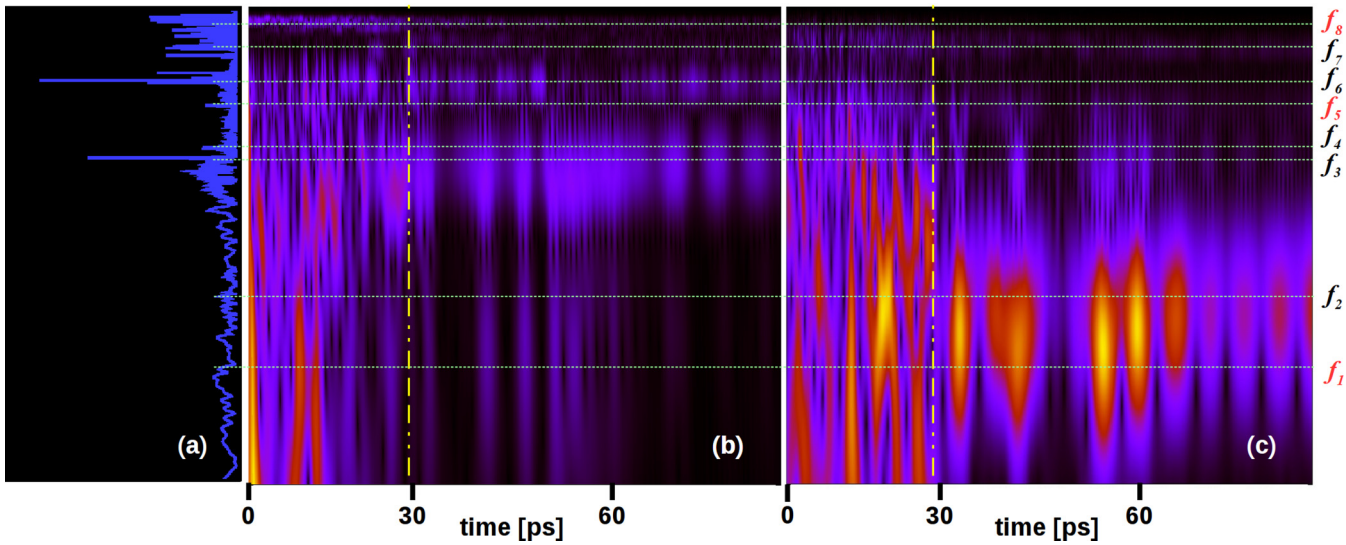

FIG. 3. (a) Fourier transform (a.u.) of the total kinetic energy at 300 K as calculated from the molecular dynamics simulation; frequency range [THz] is vertically oriented in correspondence of the frequency axis of the wavelet transform of the (b) kinetic energy and (c) the force acting on the layer A. Black-blue-red-yellow color gradient indicates increasing wavelet amplitude (a.u.). The dot-dashed vertical yellow lines represent the time $t^* \approx 29.5$ ps at which the layer sliding terminates; for $0 < t < t^*$, dissipation processes involving the sliding modes are predominant. Frequency characterization is indicated with labels in correspondence of the horizontal dotted green lines as follow: $f_1 = 1.09$, $\omega_{12} - \omega_{4,5}$; $f_2 = 1.28$, $\omega_{4,5}$; $f_3 = 2.37$, ω_{12}; $f_4 = 2.56$, $2\omega_{4,5}$; $f_5 = 3.65$, $2\omega_{4,5} + \omega_{12}$; $f_6 = 4.74$, $2\omega_{12}$; $f_7 = 8.5$, $\omega_{113,114}$; $f_8 = 26.6$, $\omega_{208,209} + \omega_{324}$. Frequencies f_1, f_5 and f_8 are generated by scattering processes among sliding [$\Gamma(4, 5)$, $\Gamma(208, 209)$] and dissipative modes [$\Gamma(12)$, $\Gamma(324)$].

then reduced to the study of the interaction between the sliding and the dissipative modes toward which the energy of the former is transferred. The recombination processes involving the sliding and dissipative modes reveal their presence with a dominant frequency contribution with the characteristic anharmonic frequencies already identified in the Fourier analysis [Fig. 3(a)]. If we resolve in time the frequency content of the energy along the sliding trajectory, we are then able to find when the dissipative processes are predominant and relate their activity to the geometric and energetic features. To this aim, we perform a wavelet transform analysis (see the Sec. S4 of the Supplemental Material [32]) of the total energy E along the entire trajectories [Fig. 3(b)]. The wavelet analysis tells us which is the frequency distribution which characterizes the energy E at each time t. First, we note that the wavelet transforms have peculiar characteristics which do not depend on the temperature; moreover, kinetic and potential energy spectrograms show the same features, thus indicating that both forms of energy are involved into the sliding and dissipation processes. Irrespective of the temperature, it is possible to divide the spectrograms into two regions: one in which the layer sliding is active and one in which it is over. The region of active sliding is dominated by the frequencies of the sliding modes and those relative to main anharmonic effects; on the contrary, once the sliding is over, the sliding frequencies have negligible contribution to the spectrograms. A close comparison between the evolution of the potential energy as calculated from the simulation and the corresponding wavelet spectrogram shows that energy dissipation is larger for those geometric configurations corresponding to the neighborhood of a local potential energy maximum. This is consistent with the fact that anharmonic scattering processes are more effective when atoms are far from their equilibrium position; correspondingly, forces acting on the A layer show a predominant anharmonic character and are not conservative if such anharmonicity is dominated by recombination processes which decrease the energy of the sliding modes. Indeed, the dissipative features that we find in the spectrogram of the kinetic and potential energy are also found in the spectrogram of the force acting on the A layer [Fig. 3(c)], further confirming that the layer deceleration is due to phonon recombination between sliding and dissipative modes. Dissipation is therefore more effective in correspondence of potential energy maxima; the study of dissipation processes is able to reveal the features of the underlying potential energy landscape. Indeed, in the next section we will show that this aspect can be exploited to get information on the energetic of the system from experimental techniques like AFM.

All the forces producing a deceleration of the layer are of frictional kind, hindering the layer drift. Since the layer sliding is active as long as the sliding modes are populated enough, *the frictional forces are all those forces which activate dissipative processes producing a depopulation of the sliding modes*. The variation of the energy of the sliding modes can then be considered equal to the work done by the frictional forces. The decrease of the sliding mode population, hence the dissipative work, is due to scattering processes which occur at a transition rate $\mathcal{P}^{j''}_{jj'}$, the latter being proportional to the product of the phonon populations involved in the scattering and to the square of the interaction strength [34]:

$$\mathcal{P}^{j''}_{jj'} \propto nn'(n''+1)|\Phi_{jj'j''}|^2. \tag{6}$$

The phonon populations n, n', and n'' vary with the time according to Eq. (2) and are a dynamic characteristic of the system: they depend from the initial conditions and from any external perturbation acting on them during the sliding (i.e., contact with a thermal reservoir, external forces). The interaction strength $\Phi_{jj'j''}$ is instead an intrinsic characteristic of the system, since it is a function of the third order force constants, the eigenfrequencies and the eigenvectors of the dynamical matrix. The frictional forces therefore depend on extrinsic properties (phonon population) which vary upon external intervention, and intrinsic properties (atomic type and geometry), which are decided once and for all when the material is built. It is therefore possible to predict the frictional response of the material by calculating the interaction strength matrix of the stable geometry and no dynamic simulations are needed. However, if the calculation of the $\Phi_{jj'j''}$ matrix elements is computationally too expensive or unfeasible, frictional dissipation processes can be studied by simulating sliding trajectories and analyzing the energy contributions by means of Eq. (5).

The protocol outlined so far is then able to identify the dissipation channels. The relation between the interaction strength governing specific phonon recombination processes, the atomic type and geometry can be found by means of collective descriptors like bond covalency [35], cophonicity [27], orbital polarization [36], and group-theory-based geometry decomposition [37,38], among others. Such descriptors are then able to suggest what are the proper atomic species and structural topologies to control the dissipation channels ultimately allowing us to design tribological materials with finely tuned frictional response at the nanoscale.

D. Atomic force microscopy signal analysis

It has been recently shown [39] that frequency analysis of the AFM signal is of great potential in providing valuable information on the atomic interactions and system response to external stimuli. We extend this suggestion by applying the protocol we described above to extract information on dissipative processes and the position of the maxima in the underlying potential from AFM measurements. To this aim, we will compare results from AFM experiments that we performed on a MoS_2 sample with molecular dynamics simulations on the bilayer system considered before. The signal recorded during AFM measurements is related to the force experienced by the AFM tip while moving on the surface sample, the latter being fixed on a substrate. The AFM scan is performed along a fixed direction and at a constant velocity. From AFM experiments, a few properties only (typically force profiles) can be directly measured. To conduct a more thorough analysis of the slip event, we performed a second set of MD simulations by considering an external force acting on the outermost S atoms of the A layer such that the velocity of those atoms is constant along the x direction; the outermost S atoms of the other layer are kept fixed during the entire simulation, resembling the adhesion of the deposited layer to

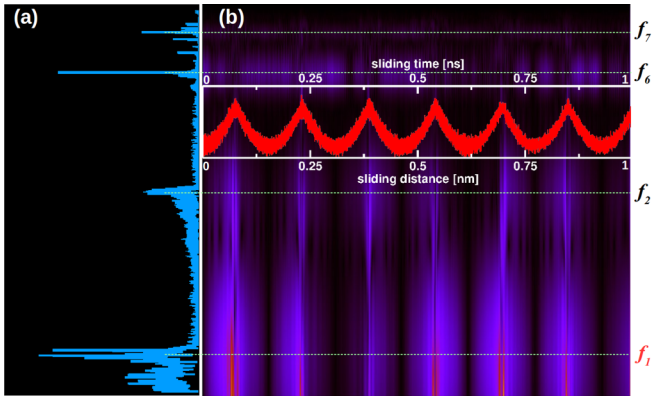

FIG. 4. (a) Fourier transform of the force acting on layer *A* at 300 K as calculated from the molecular dynamics simulation in the presence of an external force; frequency range [THz] is vertically oriented in correspondence of the frequency axis of the (b) wavelet transform of the force acting on *A*. Frequency labels and color code have the same meaning as in Fig. 3; the f_1 frequency represents the main dissipative process. Highest dissipation is found in a neighborhood of potential energy maxima (plot in the inset).

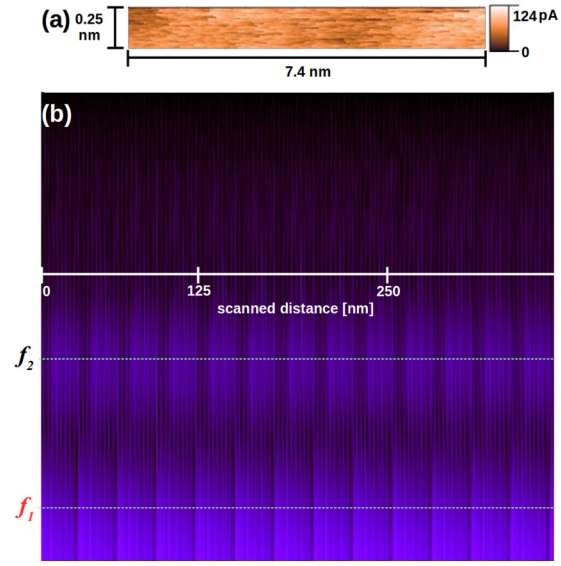

FIG. 5. (a) AFM signal and (b) corresponding wavelet transform. Two main frequency components are immediately apparent and their features are similar to those of f_1 and f_2 frequencies reported in Fig. 4. The lowest frequency can be attributed to dissipative processes active during the relative motion between the sample and the slider, and mainly present during the stick-slip event.

the substrate in the AFM experiment. Molecular dynamics trajectories have been computed at 8 different temperature values, these being 0, 50, 100, 200, 300, 400, 500, and 800 K, respectively.

To make comparisons with the lateral force signal of the AFM experiment, we will consider the force acting on the center of mass of the layer *A*. Irrespective of the temperature, the Fourier analysis of the forces [Fig. 4(a)] show features similar to the previous case [Fig. 3(a)]. The frequency spectra display the characteristic peaks of the system eigenfrequencies and dissipation processes as discussed above. The wavelet spectrograms reveal the characteristic dissipative features which appear in correspondence of the potential energy maxima [Fig. 4(b)]. We find a characteristic length of 1.6 Å, which is the periodicity of the potential energy experienced by the layer *A*. We then consider the lateral force signal from the AFM measurements. The acquired data is the outcome of a line-by-line scan on a selected rectangular region of the sample [Fig. 5(a)], and collected as a rectangular matrix, where each row corresponds to a scanned line. We then considered the matrix rows in sequence and created an *X*-*Y* set of data where *X* is the acquisition time and *Y* is the corresponding AFM data from the row. Since the scanning speed is constant, there is a linear relation between the acquisition time and the scanned distance. We then performed a wavelet analysis on such *X*-*Y* dataset and reported the spectrogram in Fig. 5(b). In this, we observe the characteristic dissipative features in place during the slip event, as we found in the force spectrogram of the MD simulations. The Fourier (not shown) and wavelet analyses point to a periodicity of the potential energy of 1.4 Å, in good agreement with the potential periodicity extracted from the simulations, also indicating comparable conditions in terms of layer commensurability and sliding directions. This result shows how our analysis is able to finely characterize the AFM signal and that a lot of information can be gathered from the AFM technique, more than what is usually done (i.e., jump lengths, maximum and average lateral forces).

IV. DISCUSSION

The characterization of the dissipative processes requires the evaluation of anharmonic effects on the system energy and, thus, on the forces. At the atomic level, such dissipative processes are described in terms of scattering among the sliding and dissipative phonon modes. The atomic description of the dissipation then requires the calculation of the phonon interaction strength $\mathbf{\Phi}$; this latter, in turns, requires the computation of third-order force constants. Such force constants are evaluated on supercells the dimensions of which can be very large compared to the unit (in general nonprimitive) cell used in dynamics simulations; such evaluation can thus be computationally highly demanding, if not prohibitive, even when the forces are evaluated by means of classical force fields. The approximation we provide in Eq. (5) is a way to circumvent this issue, because it represents a powerful tool to evaluate the anharmonic contributions to the potential energy in terms of the phonon description without the need to explicitly calculate the third-order force constants.

The geometric projection of the atomic motion onto the phonon displacement patterns is able to provide information on which are the relevant phonon distortions leading the layer drift; in this way, we are able to identify the *sliding modes*. The energy decomposition into sliding and nonsliding modes is crucial to monitor the evolution of the sliding dynamics and to identify the energy thresholds to overcome to obtain a drift of the layer. Moreover, the decomposition scheme that we have presented can also be used to provide a detailed atomic description on how the internal degrees of freedom of the system couple with the environment, usually described by *ad hoc* parametrizations (e.g., thermostats in MD simulations, damping coefficient γ in the Prandtl-Tomlinson model, etc.),

which are system-dependent and, thus, hardly transferable to the study of similar materials. The scattering processes produce a decrease of the sliding mode energy with the time, described by the transition rate at which the phonon recombinations occur; such rate, in turn, depends on both extrinsic and intrinsic parameters. The former are collectively represented by the phonon populations, which are dynamical variables that may depend on external perturbations; the latter are described by the phonon-phonon interaction strength matrix $\mathbf{\Phi}$ which is defined by the atomic kind and geometric topology of the stable geometry. The interaction strength matrix $\mathbf{\Phi}$, calculated at the geometric configuration realizing a minimum of the total energy, then governs the dissipation far from the equilibrium.

The energy loss from the sliding modes manifests itself as frictional forces producing the deceleration of the layer drift and a corresponding fingerprint of the potential energy landscape. In fact, the energy dissipation is larger in a neighborhood of the potential energy maxima; the time resolution of dissipative patterns then allows to identify which are the geometric configurations realizing critical values of the energy dissipation. This kind of analysis can be applied to characterize signals coming from any kind of experiments involving dissipative processes, like the discussed case of AFM.

Since the interaction strength matrix is the intrinsic key feature which determine dissipative phenomena, by finding the relation between the $\Phi_{jj'j''}$ matrix elements, the atomic type and the geometry, it is possible to engineer frictional properties at the nanoscale. A promising avenue is represented by collective descriptors such as bond covalency [35,40], cophonicity [27], orbital polarization [36,41], and group-theory-based geometry decomposition [37,38]; indeed, we showed how such descriptors are able to parametrize the chemical composition and geometric structure constituting a guide to design nanoengineered materials with targeted properties [27,30,40]. These results can also be exploited to control heat flux by turning on and off opportune relaxation channels, boosting the development of alternative anisotropic thermal and tribological materials.

ACKNOWLEDGMENTS

This work has been done with the support of the Czech Science Foundation (Grants No. 17-24164Y and No. 16-11516Y). This work was supported by European Regional Development Fund in the frame of the projects "Centre of Advanced Applied Sciences" (Grant No. CZ.02.1.01/0.0/0.0/16_019/0000778) and "Novel nanostructures for engineering applications" (Grant No. CZ.02.1.01/0.0/0.0/16_026/0008396). This work was supported by The Ministry of Education, Youth and Sports from the Large Infrastructures for Research, Experimental Development and Innovations project "IT4Innovations National Supercomputing Center—LM2015070." This work was partly supported by COST Action MP1303. The AFM measurements occurred in the frame of the LNSM infrastructure. We acknowledge Stanislav Leesment and Andrey Gruzdev from NT-MDT Spectrum Instruments for automation script creation. The use of VESTA [42] software is also acknowledged.

A.C. and P.N. equally contributed to derive the theoretical framework and to setup, run, and analyze the molecular dynamics simulations. K.S. deposited the MoS_2 sample and, together with E.U., performed the AFM measurements. All authors contributed to the manuscript writing.

[1] L. Prandtl, Ein gedankenmodell zur kinetischen theorie der festen körper, ZAMM-J. Appl. Math. Mech./Z. Angew. Math. Mech. **8**, 85 (1928).

[2] G. A. Tomlinson, CVI. A molecular theory of friction, London, Edinburgh, Dublin Philos. Mag. J. Sci. **7**, 905 (1929).

[3] V. L. Popov and J. A. T. Gray, Prandtl-Tomlinson model: History and applications in friction, plasticity, and nanotechnologies, ZAMM-J. Appl. Math. Mech./Z. Angew. Math. Mech. **92**, 683 (2012).

[4] A. Socoliuc, R. Bennewitz, E. Gnecco, and E. Meyer, Transition from Stick-Slip to Continuous Sliding in Atomic Friction: Entering a New Regime of Ultralow Friction, Phys. Rev. Lett. **92**, 134301 (2004).

[5] S. Y. Krylov and J. W. M. Frenken, The physics of atomic-scale friction: Basic considerations and open questions, Phys. Status Solidi (b) **251**, 711 (2014).

[6] O. Y. Fajardo, E. Gnecco, and J. J. Mazo, Anisotropy effects and friction maps in the framework of the 2d PT model, Physica B: Condens. Matter **455**, 44 (2014).

[7] G. Levita, A. Cavaleiro, E. Molinari, T. Polcar, and M. C. Righi, Sliding properties of MoS_2 layers: Load and interlayer orientation effects, J. Phys. Chem. C **118**, 13809 (2014).

[8] A. Vanossi, N. Manini, M. Urbakh, S. Zapperi, and E. Tosatti, Colloquium: Modeling friction: From nanoscale to mesoscale, Rev. Mod. Phys. **85**, 529 (2013).

[9] J. M. Martin, C. Donnet, T. Le Mogne, and T. Epicier, Superlubricity of molybdenum disulphide, Phys. Rev. B **48**, 10583 (1993).

[10] B. Radisavljevic, A. Radenovic, J. Brivio, V. Giacometti, and A. Kis, Single-layer MoS_2 transistors, Nat. Nanotechnol. **6**, 147 (2011).

[11] X.-R. Shi, H. Jiao, K. Hermann, and J. Wang, CO hydrogenation reaction on sulfided molybdenum catalysts, J. Mol. Catal. A: Chem. **312**, 7 (2009).

[12] S. J. Plimpton, Fast parallel algorithms for short-range molecular dynamics, J. Comput. Phys. **117**, 1 (1995).

[13] J.-W. Jiang, H. S. Park, and T. Rabczuk, Molecular dynamics simulations of single-layer molybdenum disulphide (MoS_2): Stillinger-Weber parametrization, mechanical properties, and thermal conductivity, J. Appl. Phys. **114**, 064307 (2013).

[14] B. Schönfeld, J. J. Huang, and S. C. Moss, Anisotropic mean-square displacements (MSD) in single-crystals of 2H- and 3R-MoS_2, Acta Crystallogr. B **39**, 404 (1983).

[15] S. Nosé, A unified formulation of the constant temperature molecular dynamics methods, J. Chem. Phys. **81**, 511 (1984).

[16] W. G. Hoover, Canonical dynamics: Equilibrium phase-space distributions, Phys. Rev. A **31**, 1695 (1985).

[17] A. Togo and I. Tanaka, First principles phonon calculations in materials science, Scripta Materialia **108**, 1 (2015).

[18] J. Zekonyte and T. Polcar, Friction force microscopy analysis of self-adaptive W-S-C coatings: Nanoscale friction and wear, ACS Appl. Mater. Interfaces **7**, 21056 (2015).

[19] J. Zekonyte, A. Cavaleiro, and T. Polcar, Frictional properties of self-adaptive chromium doped tungsten-sulfur-carbon coatings at nanoscale, Appl. Surf. Sci. **303**, 381 (2014).

[20] F. Gustavsson, M. Bugnet, T. Polcar, A. Cavaleiro, and S. Jacobson, A high-resolution TEM/EELS study of the effect of doping elements on the sliding mechanisms of sputtered WS_2 coatings, Tribol. Trans. **58**, 113 (2014).

[21] F. Gustavsson, S. Jacobson, A. Cavaleiro, and T. Polcar, Ultra-low friction W-S-N solid lubricant coating, Surf. Coat. Technol. **232**, 541 (2013).

[22] T. Polcar, F. Gustavsson, T. Thersleff, S. Jacobson, and A. Cavaleiro, Complex frictional analysis of self-lubricant W-S-C/Cr coating, Faraday Discuss. **156**, 383 (2012).

[23] J. Kerssemakers and J. T. M. De Hosson, Atomic force microscopy imaging of transition metal layered compounds: A two-dimensional stick-slip system, Appl. Phys. Lett. **67**, 347 (1995).

[24] E. Gnecco and E. Mayer, *Fundamentals of Friction and Wear* (Springer-Verlag, Berlin, 2007), p. 101.

[25] J. E. Sader, J. W. M. Chon, and P. Mulvaney, Calibration of rectangular atomic force microscope cantilevers, Rev. Sci. Instrum. **70**, 3967 (1999).

[26] J. E. Sader, I. Larson, P. Mulvaney, and L. R. White, Method for the calibration of atomic force microscope cantilevers, Rev. Sci. Instrum. **66**, 3789 (1995).

[27] A. Cammarata and T. Polcar, Tailoring nanoscale friction in MX_2 transition metal dichalcogenides, Inorg. Chem. **54**, 5739 (2015).

[28] A. Cammarata and T. Polcar, Electro-vibrational coupling effects on "intrinsic friction" in transition metal dichalcogenides, RSC Adv. **5**, 106809 (2015).

[29] A. Cammarata and T. Polcar, Layering effects on low frequency modes in n-layered MX_2 transition metal dichalcogenides, Phys. Chem. Chem. Phys. **18**, 4807 (2016).

[30] A. Cammarata and T. Polcar, Overcoming nanoscale friction barriers in transition metal dichalcogenides, Phys. Rev. B **96**, 085406 (2017).

[31] Indeed, the lattice distortions associated to the phonon modes at the Γ point of the reciprocal space of the simulated geometry are the only ones which can be sampled in a dynamic simulation, due to the following reason. In molecular dynamics simulations, atomic positions are evaluated in the direct (real) space; it is then possible to sample only those lattice distortions associated to phonon waves the wavelength of which is contained within the simulation box. Any geometric distortion associated to a wave with a wavelength greater than the dimensions of the system would not satisfy the periodic boundary conditions, and therefore cannot be sampled. In general, to sample a wave described by a vector $\boldsymbol{k}^* = (1/l,\ 1/m,\ 1/n)$ of the reciprocal space of a primitive unit cell, it is necessary to run a dynamic simulation using the corresponding $l \times m \times n$ supercell geometry. Since, by definition, such geometry does not represent a primitive unit cell, the vector $\boldsymbol{k}^*$ will be refolded onto the Γ point of the corresponding reciprocal lattice.

[32] See Supplemental Material at http://link.aps.org/supplemental/10.1103/PhysRevB.99.094309 for schemtics of the sliding modes, the formal derivation of the projection of the system's state onto the normal modes, the approximated expression for calculating the potential energy with corrections up to the third order, and more information on the wavelet transform analysis.

[33] D. M. Wallace, *Thermodynamics of Crystals* (John Wiley & Sons, New York, 1972).

[34] J. M. Ziman, *Electrons and Phonons: The Theory of Transport Phenomena in Solids*, The international series of monographs on physics (Oxford University Press, Oxford, 1960), p. 135.

[35] A. Cammarata and J. M. Rondinelli, Covalent dependence of octahedral rotations in orthorhombic perovskite oxides, J. Chem. Phys. **141**, 114704 (2014).

[36] A. Cammarata and J. M. Rondinelli, Octahedral engineering of orbital polarizations in charge transfer oxides, Phys. Rev. B **87**, 155135 (2013).

[37] B. J. Campbell, H. T. Stokes, D. E. Tanner, and D. M. Hatch, ISODISPLACE: A web-based tool for exploring structural distortions, J. Appl. Crystallogr. **39**, 607 (2006).

[38] D. Orobengoa, C. Capillas, M. I. Aroyo, and J. M. Perez-Mato, AMPLIMODES: Symmetry-mode analysis on the Bilbao crystallographic server, J. Appl. Crystallogr. **42**, 820 (2009).

[39] V. Pukhova and G. Ferrini, Multi-frequency data analysis in AFM by wavelet transform, IOP Conf. Ser.: Mater. Sci. Eng. **256**, 012004 (2017).

[40] A. Cammarata, W. Zhang, P. S. Halasyamani, and J. M. Rondinelli, Microscopic origins of optical second harmonic generation in noncentrosymmetric-nonpolar materials, Chem. Mater. **26**, 5773 (2014).

[41] A. Cammarata and J. Rondinelli, Microscopic interactions governing phase matchability in nonlinear optical materials, J. Mater. Chem. C **4**, 5858 (2016).

[42] K. Momma and F. Izumi, *VESTA*: A three-dimensional visualization system for electronic and structural analysis, J. Appl. Cryst. **41**, 653 (2008).